

Complex Quasiparticle Band Structure Induced by Electron-Phonon Interaction: Band Splitting in the 1×1 H/W(110) Surface

Asier Eiguren^{1,2} and Claudia Ambrosch-Draxl¹

¹*Chair of Atomistic Modelling and Design of Materials, University of Leoben, Franz-Josef-Straße 18, A-8700 Leoben, Austria*

²*Donostia International Physics Center (DIPC), Paseo Manuel de Lardizabal 4, E-20018 Donostia/San Sebastian, Spain*

(Received 29 January 2007; revised manuscript received 12 September 2007; published 18 July 2008)

We show that the self-consistent solution of the complex Dyson equation for the electron-phonon (EP) problem introduces many body effects which are often observed in photoemission experiments. The formalism is applied to the H covered W(110) surface, using first-principles results for the electronic and vibrational structure. We demonstrate that the measured spin-polarized surface band splitting [Phys. Rev. Lett. **84**, 2925 (2000); **89**, 216802 (2002)] can be traced back to different quasiparticle (QP) states induced by EP coupling. Despite the breakdown of the single QP picture, the spectral functions are very well represented by the predicted multiple QP structure.

DOI: [10.1103/PhysRevLett.101.036402](https://doi.org/10.1103/PhysRevLett.101.036402)

PACS numbers: 71.38.Cn, 71.10.-w, 79.60.-i

Recent developments in angle-resolved photoemission spectroscopy (ARPES), revealing subtle details of the electronic structure, pose a challenge for a proper theoretical interpretation. In particular, many 2D systems exhibit peculiarities in the measured spectral functions, being far from the ideal Lorentzian shape. Such observations include materials as different as bulk graphite [1] and high- T_c cuprates [2]. One possible origin can be found in electron-phonon (EP) coupling. This interaction is usually more pronounced in low dimensions, and the understanding of EP related phenomena has gained a lot of interest from the experimental as well as theoretical side during the last years [3–10]. One of the most prominent systems in this context is the hydrogen covered W(110) surface: For one of the surface states, experiment [7] indicates the occurrence of two clear structures in the ARPES spectra, both with well defined energy dispersion. Thereby, isotope substitution provided striking evidence for EP interaction [7] being the source for the band splitting. The fact that the surface states are spin polarized as well as spin-orbit (SO) split [11], adds more interesting features to this already puzzling situation. In this Letter, we show that EP interaction indeed leads to multiple quasiparticle (QP) states. By following an idea of Engelsberg and Schrieffer (ES) [12,13], but extending this work to finite temperatures and by combining it with *ab initio* calculations based on density functional theory (DFT), we obtain self-consistently renormalized QP energy bands and lifetimes. Application to the 1×1 H/W(110) surface demonstrates that several QP states are present, offering an explanation for the experimentally observed band splitting.

We modeled this system by a slab consisting of seven tungsten layers plus one additional H layer on each surface. The first-principles part of our calculations was carried out in the framework of DFT, applying the local-density approximation within the pseudopotential approach utilizing the PWSCF code [14]. We first performed scalar-relativistic non-spin-polarized calculations for the surface

relaxation [15], and as a next step, we included spin-orbit coupling thereby introducing spinor wave functions. The Fermi surface of the slab system is shown in Fig. 1. We find two SO split surface states around the S point (labeled S_1 and S_2), perfectly reproducing spin-polarized photoemission measurements [11]. These states form an effective two-dimensional electron gas strongly interacting with phonons. In the right panel the electron band structure is displayed along $\bar{\Gamma}\bar{S}$, where the gray area indicates the projected bulk bands. The red dots highlight the two surface bands, S_1 and S_2 , avoiding band crossings. These bands are in excellent agreement with experiments in terms of dispersion and splitting [11].

In Fig. 2 we show the vibrational spectra calculated without including SO coupling. The lower phonon bands (<30 meV) basically correspond to tungsten displacements while the three highest vibrational modes involve mostly hydrogen. Their frequencies and the mode assignment fully agree with experiments [17–19], labelling them as the wagging mode (~ 100 meV), and the asymmetric

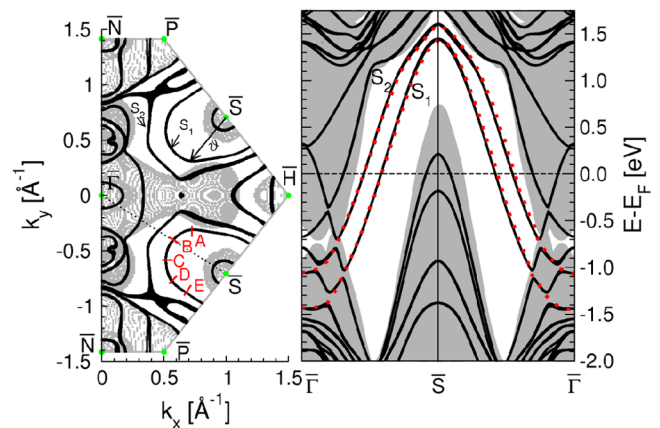


FIG. 1 (color online). Left: Fermi surface of the slab system. Right: Electron bands along $\bar{\Gamma}\bar{S}$, the gray area indicating the projected bulk bands. Red dots highlight the S_1 and S_2 bands.

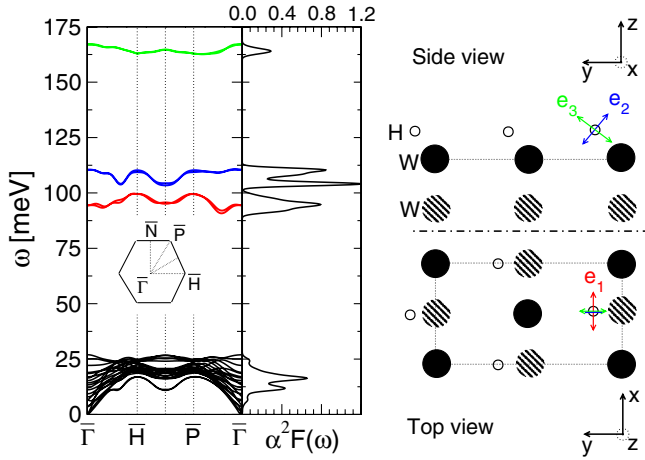


FIG. 2 (color online). Left: Phonon band structure and the Eliashberg function of the S_1 state in $\bar{\Gamma}\bar{S}$ direction. Right: Side and top view of the surface indicating the eigenvectors of the three hydrogen modes.

(~ 110 meV) and symmetric (~ 160 meV) stretch modes. The corresponding polarization vectors \mathbf{e}_1 , \mathbf{e}_2 and \mathbf{e}_3 (ordered by increasing energy) are schematically represented in the right panel of the figure. To obtain the Eliashberg functions, we have considered a $40 \times 40 \times 1$ grid for both, electron and phonon wave vectors, where the EP matrix elements $g_{\mathbf{q},\mathbf{k},\nu} = \sum_{\sigma,\sigma'} \langle \psi_{\sigma',\mathbf{q}+\mathbf{k}} | \delta V_{\mathbf{q},\nu} | \psi_{\sigma,\mathbf{k}} \rangle \delta_{\sigma,\sigma'}$ have been evaluated by considering the full spinor states. The middle panel of Fig. 2 shows the calculated Eliashberg function for the surface band S_1 along the $\bar{\Gamma}\bar{S}$ direction.

In the following, we sketch the procedure to obtain *ab initio* QP excitations in a self-consistent manner. To start with, we describe the many body effects induced by EP interaction through the electron self-energy, where this quantity is treated within second order perturbation theory [20]:

$$\Sigma_{\mathbf{k}}(E) = \int 2\Sigma^{Ei}(E, \omega) \alpha^2 F_{\mathbf{k}}(\omega) d\omega, \quad (1)$$

$$\Sigma^{Ei}(E, \omega) \equiv \frac{1}{2} \int_{-\infty}^{\infty} \left[\frac{n(\omega) + 1 - f(\nu)}{E - \nu - \omega} + \frac{n(\omega) + f(\nu)}{E - \nu + \omega} \right] d\nu. \quad (2)$$

Thereby Σ^{Ei} is the self-energy in the Einstein model, which is characterized by the interaction of an electron with a single phonon, with energies E and ω , respectively. f and n denote the Fermi and Bose distributions. The energies and lifetimes of the QP excitations are provided by the complex poles of the electron Green function $G_{\mathbf{k}}(z) = 1/(z - \epsilon_{\mathbf{k}}^0 - \Sigma_{\mathbf{k}}(z))$. Simply replacing real energies, E , by their complex counterparts, z , in Eq. (2) would lead to a discontinuous Green function across the real axis. Therefore the poles in the complex plane must be found by analytic continuation of $\Sigma(z)$ from the upper to the lower half plane [12,21]. We obtain the continuation of $G(z)$, i.e., $\tilde{G}(z)$, through the continuation of $\Sigma^{Ei}(z)$,

$$\tilde{\Sigma}^{Ei}(z, \omega) = -i\pi \left(n(\omega) + \frac{1}{2} \right) + \frac{1}{2} \Psi \left(\frac{1}{2} + i \frac{\omega - z}{2\pi T} \right) - \frac{1}{2} \Psi \left(\frac{1}{2} - i \frac{\omega + z}{2\pi T} \right), \quad (3)$$

in terms of the Digamma function Ψ [22]. This function fulfills all the analytic requirements [23]. As a consequence, the proper Dyson equation reads

$$\tilde{\xi}(z) \equiv \tilde{G}(z)^{-1} = z - \epsilon_{\mathbf{k}}^0 - \tilde{\Sigma}_{\mathbf{k}}(z) = 0, \quad (4)$$

where $\tilde{\Sigma}_{\mathbf{k}}(z)$ and $\tilde{\Sigma}^{Ei}(z)$ are given by Eqs. (1) and (3), respectively, [but not Eq. (2)]. This is our basic equation to describe the electronic excitations. Our procedure to obtain the exact QP poles of $\tilde{G}(z)$ is the following: Given the bare electron energy $\epsilon_{\mathbf{k}}^0$, we search for the possible complex values $z = E_{\mathbf{k}}^{\text{qp}} = E_R(\mathbf{k}) + iE_I(\mathbf{k})$ satisfying Eq. (4), where $E_R(\mathbf{k})$ and $E_I(\mathbf{k}) \equiv 1/\tau$ represent the fully renormalized QP energy and inverse lifetime, respectively. Note that Eq. (4) implies two equations, i.e., $E_R = \epsilon_{\mathbf{k}}^0 + \text{Re}[\tilde{\Sigma}_{\mathbf{k}}(E_R, E_I)]$ and $E_I = \text{Im}[\tilde{\Sigma}_{\mathbf{k}}(E_R, E_I)]$, that need to be solved self-consistently. We will demonstrate below that the full solution of Eq. (4) naturally gives rise to multiple poles, i.e., several solutions for the same electron wave vector \mathbf{k} . The most common approximation for Eq. (4) is to consider the imaginary part of the self-energy directly as the inverse lifetime, $1/\tau_{\mathbf{k}}^0 = E_I^0(\mathbf{k}) \equiv \text{Im}[\tilde{\Sigma}_{\mathbf{k}}(E_R^0(\mathbf{k}), E_I = 0)]$ and this equation is evaluated at approximate QP energies, E_R^0 , which are obtained by neglecting the effect of all imaginary components in the Dyson equation [Eq. (4)], i.e., by solving

$$E_R^0(\mathbf{k}) = \epsilon_{\mathbf{k}}^0 + \text{Re}[\tilde{\Sigma}_{\mathbf{k}}(E_R^0(\mathbf{k}), E_I = 0)]. \quad (5)$$

This is the most popular way to estimate QP energies and lifetimes. The shortcoming that E_I as well as the renormalization of the electron bands due to E_R are neglected above, can be partly compensated by considering a Taylor expansion of Eq. (4) around E_R^0 [6,20], $1/\tau_{\mathbf{k}}^1 = E_I^1 = Z_{\text{qp}}(E_R^0) \text{Im}[\tilde{\Sigma}_{\mathbf{k}}(E_R^0, E_I = 0)]$. This is the well-known *quasi-particle expansion*, where $Z_{\text{qp}}(z) \equiv 1/(1 - \Sigma'(z))$ is the so called quasiparticle renormalization factor. The problem with this procedure is that it gives unphysical results even for moderate EP coupling, since Z_{qp} diverges for $\Sigma' \sim 1$. In contrast, the self-consistent solution of the complex Dyson equation solves this problem and goes beyond the procedure considered in Ref. [6].

We now evaluate the above discussed quantities for the H/W(110) surface system. The real part of the self-energy is depicted in Fig. 3 (left panel) for $T = 0$ K and $T = 150$ K. To compare with the photoemission measurements [8] we have chosen similar directions (A-E, as indicated in Fig. 1). Our calculations show a weaker anisotropy than the one observed in Ref. [8], but the trends are reproduced, with a maximum of interaction around slices C and D and decreasing when going towards A and E, respectively. This behavior is underpinned by the angular dependence of the

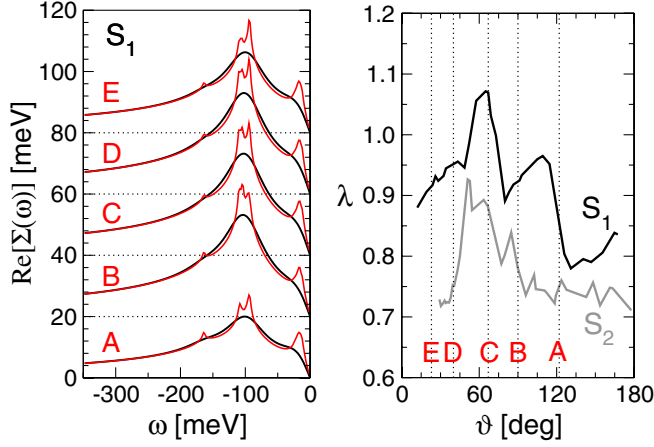


FIG. 3 (color online). Left: Real part of the self-energy at $T = 0$ K (red) and $T = 150$ K (black) along the slices A-E. Right: Angular dependence of the EP parameter λ for the surface states S_1 and S_2 . For definitions of A-E and the angle ϑ see Fig. 1.

EP coupling parameter λ , which is shown in the right panel. Along the $\bar{\Gamma}\bar{S}$ direction, we find $\lambda_{\bar{\Gamma}\bar{S}} \sim 0.9$ for S_1 , which is in the range of measured values, i.e., between 0.8 to 1.4 [7,8]. For S_2 , the $\lambda_{\bar{\Gamma}\bar{S}}$ value of ~ 0.8 is weaker than for S_1 but considerably stronger than for the bulk states for which we find $\lambda \sim 0.25$ – 0.45 . For this direction, the shape of calculated and experimentally inferred $\text{Re}\Sigma$ [8,10] are in very good agreement, where we confirm a pronounced structure at ~ 100 – 110 meV originating from the wagging and the asymmetric-stretch modes exclusively, but not from the symmetric-stretch mode [10]. We also resolve the experimentally observed shoulder at 20 meV which we trace back to tungsten vibrations. The low-energy substrate phonons participate substantially, i.e., with $\sim 70\%$ to the total mass enhancement at the Fermi level. The wagging and the asymmetric stretch modes contribute each with $\sim 15\%$, while the effect of the stretching mode is negligible. In contrast, electrons close to $E \sim 100$ eV are renormalized almost exclusively by the wagging and the asymmetric stretch modes. The latter goes in hand with the finding that the symmetric-stretch mode cannot be responsible for the shape of the real part of the self-energy [10] as originally assumed [7]. Regarding the fact, that several approximations [24] had to be used for estimating the QP energies and $\text{Re}\Sigma$ from experiment, the overall agreement with experiment is very good.

In order to investigate the QP structure of the surface, we self-consistently solved Eq. (4) for the S_1 state in $\bar{\Gamma}\bar{S}$ direction, at low but finite temperatures. The solid black and gray lines in the left panels of Fig. 4 represent the fully renormalized QP dispersion, i.e., the real parts of the poles $E_R(\mathbf{k}, n)$ vs electron momentum \mathbf{k} at $T = 150$ K and $T = 40$ K, respectively. The background color reflects the positive part of the second derivative of the electron spectral function, $\partial^2 A_{\mathbf{k}}(\omega)/\partial \omega^2$, such that the peaks and shoulders of $A_{\mathbf{k}}(\omega)$ are highlighted. It is remarkable that most of the QP bands correspond to features in the spectral function

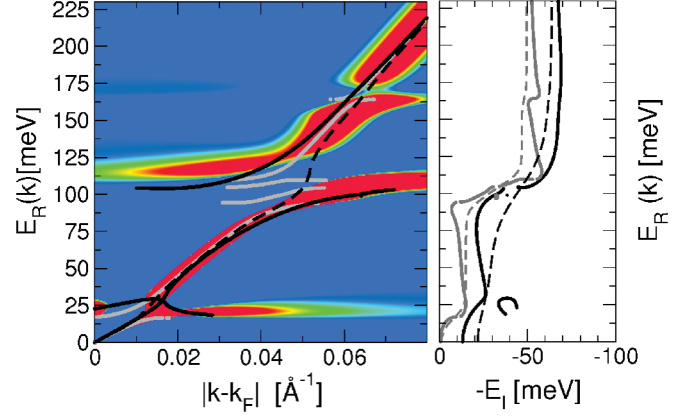


FIG. 4 (color). Self-consistent solution of the complex Dyson equation for H/W(110). Left: QP bands (solid lines) at $T = 150$ K (black) and 40 K (gray). The background color presents the second derivative of the spectral function at $T = 40$ K. Right: Inverse lifetimes $1/\tau = |E_I|$ (solid) and bare self-energies $1/\tau^0 = |\Sigma_I|$ (dashed) at $T = 40$ K (gray) and $T = 150$ K (black).

(Fig. 5) with some of the bands, however, slightly displaced. This aberration phenomena appears due to the finite lifetimes. The main experimental finding, e.g., a band splitting at ~ 100 – 150 meV, is reproduced by the QP bands, but additional QP states are predicted, which should be confirmed by experiments with higher resolution. In comparison, the dashed line corresponds to the solution of Eq. (5), the approximation ignoring all imaginary components. Note that Eq. (5) describes only one QP state per \mathbf{k} , while in our calculations several states are predicted for a given wave vector. The first energy splitting at ~ 20 meV corresponds to the main peak of $\alpha^2 F(\omega)$ in the low-energy range in Fig. 2. Electrons above ~ 20 meV are energetically allowed to emit all tungsten related pho-

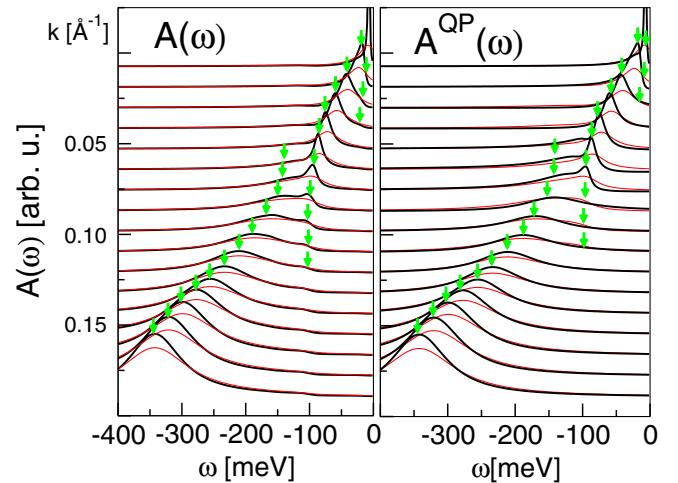


FIG. 5 (color online). Spectral functions, $A_{\mathbf{k}}(\omega)$, at $T = 40$ K (thick black) and $T = 150$ K (thin red) of H/W(110) for different momenta compared to their counterparts in the multiple quasiparticle approximation, $A_{\mathbf{k}}^{\text{QP}}(\omega)$, given by Eq. (6).

non modes ($\omega \lesssim 20$ meV), but below this energy, only virtual excitations are possible. As a consequence, the effective mass of electrons at $E \lesssim 20$ meV gets considerably enhanced, but reduced for slightly higher energies. For electron states between 20 and 90 meV there is an interplay between the real emission processes of the lowest energy phonon modes and the virtual emission processes of the vibrations highest in energy. A minor additional splitting is also predicted at ~ 160 meV, which we believe could not be detected experimentally due to finite resolution. The right panel of Fig. 4 compares the fully renormalized and bare lifetimes, i.e. $1/\tau = E_I$ (solid) and $1/\tau^0 = \text{Im}[\Sigma(E_R, 0)]$ (dashed), at $T = 40$ K (gray) and 150 K (black). One can conclude that renormalization effects significantly enhance QP lifetimes for electron energies lower than the prominent features in the Eliashberg functions. For electron energies, where the Eliashberg function is negligible, the zero order lifetime τ^0 shows a plateau behavior while the fully renormalized lifetime τ is significantly modulated.

Given the fact that the estimation of the self-energy and the QP energies from ARPES experiments need an underlying theory to rely on [commonly Eq. (5)], the most natural quantity for comparison of theory and experiment is the spectral function. At the same time the question arises whether and to which extent the predicted multiple QP states can be related to the features of the spectral functions. This is an important issue since the appearance of multiple QP states are a clear indication for the breakdown of the single QP picture. The left panel of Fig. 5 shows the calculated spectral functions at 40 and 150 K, which are indeed in very good agreement with its measured counterparts [7]. While a single QP state shows a perfect Lorentzian spectral function, here the spectral lines are more complex. To discuss this point, we consider the first term of a Laurent series around each pole and sum over all contributions

$$A_{\mathbf{k}}^{\text{QP}}(E) \equiv \sum_n \text{Im} \left[\frac{-Z^{\text{QP}}(\mathbf{k}, n)/\pi}{E - E^{\text{QP}}(\mathbf{k}, n)} \right]. \quad (6)$$

Although this function is constructed from the contributions of the QP states only, it reproduces the shape of the full spectral function ($A(E) = -\text{Im}[\tilde{G}(E)/\pi]$) remarkably well, as can be seen by comparing the two panels of Fig. 5. This fact demonstrates that, despite the break down of the single QP picture, the QP picture itself is still adequate, but only with the extension that several QP states are possible.

Compiling the comparison between theory and available experimental data, we find close agreement for both, the spin-polarized electronic structure and the vibrational properties. Similarly, the calculated self-energy, $\text{Re}\Sigma$, and the mass enhancement parameter, λ , are well described. The experimentally determined $\text{Re}\Sigma$ shows a prominent peak at ~ 100 – 110 meV, which we trace back to the wagging and the asymmetric stretch modes. The theoretically obtained anisotropy of the coupling is some-

what weaker than experimentally inferred [8], but the trend is reproduced. Moreover, the calculated spectral functions closely follow the experimental ones. With all these data at hand, a self-consistent solution of the Dyson equation can be considered reliable, finding that multiple QP poles are present, and offering an explanation for the experimentally observed band splitting. The latter is a quite general phenomenon, not specific of this surface, and not even of the 2D character. In principle, a QP band separation occurs irrespective of the magnitude of the coupling constant and the dimensionality, but it appears more dramatic when the interaction is strong, vanishing continuously as the coupling goes to zero. The precise shape of the renormalized QP bands depends on the specific Eliashberg function, but generally, the most important effects are found close to the energies where the Eliashberg function shows a prominent structure. ARPES spectra on other surfaces [3] and high T_c materials [2] exhibiting similar shapes should be explored in this respect.

Work supported by the Austrian Science Fund, Project No. P16227, and the EU (EXC!TING network, Contract No. HPRN-CT-2002-00317), *Gipuzkoako Foru Aldundia*, and DIPC (Spain). We appreciate very valuable discussions with U. Hohenester and P. M. Echenique.

-
- [1] K. Sugawara *et al.*, Phys. Rev. Lett. **98**, 036801 (2007).
 - [2] A. Lanzara *et al.*, Nature (London) **412**, 510 (2001).
 - [3] S. LaShell *et al.*, Phys. Rev. B **61**, 2371 (2000).
 - [4] A. Eiguren *et al.*, Phys. Rev. Lett. **88**, 066805 (2002).
 - [5] J. Shi *et al.*, Phys. Rev. Lett. **92**, 186401 (2004).
 - [6] A. Eiguren *et al.*, Phys. Rev. Lett. **91**, 166803 (2003).
 - [7] E. Rotenberg *et al.*, Phys. Rev. Lett. **84**, 2925 (2000).
 - [8] E. Rotenberg and S.D. Kevan, J. Electron Spectrosc. Relat. Phenom. **126**, 125 (2002).
 - [9] M. Hengsberger *et al.*, Phys. Rev. Lett. **83**, 592 (1999).
 - [10] E.W. Plummer *et al.*, Prog. Surf. Sci. **74**, 251 (2003).
 - [11] M. Hochstrasser *et al.*, Phys. Rev. Lett. **89**, 216802 (2002).
 - [12] S. Engelsberg *et al.*, Phys. Rev. **131**, 993 (1963).
 - [13] ES studied the Einstein and the Debye models at $T = 0$.
 - [14] S. Baroni *et al.*, Rev. Mod. Phys. **73**, 515 (2001).
 - [15] The hydrogen binding site is displaced from the ideal high-symmetry position by ~ 0.60 Å in y direction, in agreement with previous results [16]. The distance between the top W and H layers is ~ 1.07 Å.
 - [16] B. Kohler *et al.*, Phys. Rev. B **56**, 13 503 (1997).
 - [17] M. Balden *et al.*, Phys. Rev. Lett. **73**, 854 (1994).
 - [18] E. Hulpke *et al.*, Phys. Rev. Lett. **68**, 2846 (1992).
 - [19] Y.J. Chabal *et al.*, Phys. Rev. Lett. **55**, 845 (1985).
 - [20] G. Grimvall, *The Electron-Phonon Interaction in Metals* (North-Holland, Amsterdam, 1981).
 - [21] P. Nozieres, *Theory of Interacting Fermi Systems* (W.A. Benjamin, New York, 1964).
 - [22] P.B. Allen and B. Mitrovic, Solid State Phys. **37**, 1 (1982).
 - [23] $\tilde{\Sigma}^{Ei}(z)$ equals $\Sigma^{Ei}(z)$ only for z in the upper half plane but is continuous across the real axis.
 - [24] In Ref. [8] the approximate Eq. (5) was used to estimate QP energies and $\text{Re}\Sigma$, where the bare electron energies were inferred from fitting to a parabolic band.